Examination of additively manufactured auxetic components using a novel testing setup

Abstract. This paper reports upon the results of an initial test cycle using a bespoke testing rig designed expressly to examine additively manufactured auxetic components. Firstly, the key problems facing practical researchers in the field of auxetics is explored with the treatment of the boundary condition identified as a key issue. The testing setup that is then introduced utilises a novel means of part mounting and facilitates optical analysis and real-time force measurements. The study analyses three different auxetic structures (re-entrant, chiral and semi-rigid), a set of samples of which were additively manufactured in TPU material. A range of parameters were varied across the three designs including interior geometry and wall thicknesses in order to demonstrate the effectiveness of the setup for the examination of different structures. Several key results were distilled from the tests that were then further analysed through numerical modelling and discussed with respect to future testing. Our investigation shows a close alignment between the physical testing results and the simulations, indicating that the testing configuration is rigorous and may be used to explore the mechanical behaviour of more complex auxetic componentry.

Keywords: Auxetics; Mechanical analysis; Simulation; Additive manufacturing

1 Introduction and background

Auxetics are interesting materials that display deformation properties with a negative Poisson's ratio and have been studied extensively over the last few decades within material and engineering science [1]. Common designs include re-entrant, chiral and semi-rigid [2] (Fig 1). Testing auxetics and other deformable structures with a view to advancing understanding of the behaviour of additively manufactured parts, exploring applications or expanding the scope of possible testing strategies presents a number of challenges for researchers. Notably, control and monitoring of boundary conditions and buckling behaviour have proved to be difficult to implement rigorously due to the requirements of direct interference with the structure. For this reason, achieving setups that can replicate simulated results with reliability and accuracy is difficult. This work seeks to address some of these issues by exploring the short comings of various practical testing approaches proposed throughout the literature and presenting results from a new testing setup developed by the authors. The new testing system explores a novel method for controlling the boundary conditions to a much higher degree. Boundary conditions, i.e. the way in which the components are held or fixed at their perimeters, are a fundamental concern in this kind of mechanical testing as they affect how the properties of the overall structure respond to change such as large deformations.

Furthermore, it is to highlight that the method presented for testing auxetics structures is not explicitly addressing the derivation of mechanical properties such as strength at yield or break or Poisson's ratio. The aim is to explore a novel testing approach based on a new setup for boundary and constraints conditions under a bi-axial loading condition. This paper will be split into three key stages in which we can explore the effectiveness of the new testing approach. Firstly, we will consider the literature on physical testing approaches undertaken by other researchers examining auxetics. Secondly, the experimental work undertaken by the authors as part of a wider research project is set out. Thirdly, experimental results will be compared to numerical results, to highlight the differences between the specimen behaviour in actual experimental conditions with respect to ideal simulated conditions. The discussion of the results will then be provided, describing the effectiveness of the approach and next steps for future researchers.

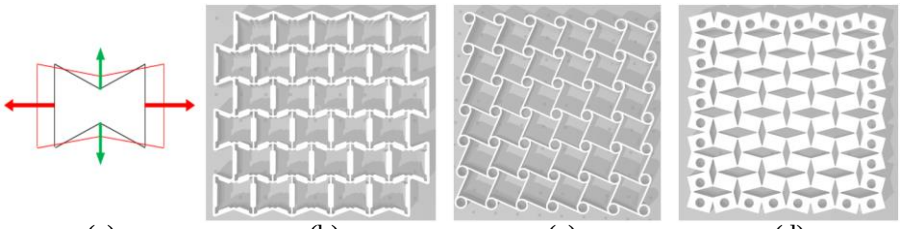

Fig. 1. Force-deformation diagram for an auxetic structure (a). Typical re-entrant (b), chiral (c) and semi-rigid (d) auxetic geometry.

2 Auxetics: Key issues in testing set-ups

2.1.1 Conventional testing setups

By definition, an auxetic is a structure that produces a negative Poisson's-ratio (NPR) in terms of its mechanical deformation when subjected to loads [1]. Within the literature focusing on the examination of 3D printed auxetic components, a number of setup variations have been identified that we could class as more conventional, requiring less advanced equipment. Work from [3] exemplifies how simple jigs can be developed in order to examine the behaviour of parts under loading. A simple configuration exploits a rudimentary cuboidal transparent plastic structure to encase the auxetic, allowing the structure to compress without buckling across the z-axis. The transparent plastic allows for examination of the part as it is compressed although there is no formalised way to assess the changes in dimensional structure. Additionally, the boundary problem is addressed only by applying a uniform pressure to the top surface; the part is not held within a vice. While this offers some practical flexibilities, it leaves open the possibilities of slippages and inaccuracies in any given analysis. Other researchers have explored the use of slightly more advanced setups with readily available componentry. There are notable examples in the literature of different methods of holding the parts within custom made jigs. Research from [4] for example used a fixed jaw and a movable jaw in conjunction with a high-speed camera for their optical analysis. Markers are

placed directly on the part to track the relative position of the points as the part is subjected to tension. The change in the relative position of the points is then interpreted by a computer, providing an assessment of how the part behaves. A similar approach was taken by [5] who examined the behaviour of thinner auxetic samples. The work used simple time lapsed photos to record the changes of the structure, resulting in a simple and effective method. [6] utilised a more thorough optical analysis method. The set up uses a jaw style jig that holds the component which is then pulled to tension using a series of rail-mounted stepper motors. The optical analysis method involves tracking the relative position of a large number of points in the structure. Interestingly, a set of nodes have been added to the core structure that are then integrated into the jig, thus allowing the central structure to behave somewhat independently, moving the boundary problem away from the section being studied directly. In another interesting setup, the authors [7] secured the sample with use of a set of supporting truss structures. The pins are placed uniformly within the auxetic structure itself. This means that the boundary condition can be more carefully controlled, and the setup potentially facilitates more complex local deformation tests although the boundary condition remains uncontrolled on two sides of the component. The researchers used a similar optical analysis method to determine the results.

2.1.2 Advanced testing setups

Beyond the optical analysis tools that are characteristic of the "conventional" testing methods, other researchers have utilised what we can categorise as more advanced methods of analysis. In work by [8] for example, an auxetic sample is mechanically tested using a low velocity hydraulic press. Used in conjunction with an accelerometer, the analysis method determines material behaviour by examining the speed rate of material compression. The boundary condition is set by uniform surface contact of the striker and the bottom plate with the sample. Other work [2] explores a less conventional approach by compressing the auxetic sample off-axis. This creates a complex boundary condition where one side of the component (in this case a 3d printed metallic part) is subjected to compression while the other side is held in a static position. In a highly developed study [9], the researchers tested a range of auxetic structures by physical experimentation and numerical analysis with FE modelling. The researchers made a number of observations including that some structures exhibited properties of high stress resistance. A similar study explored the reliability of FE modelling using SolidWorks finding mixed results: strain behaviour could be accurately predicted but forces and stresses were less accurate [10]. Another research effort [11] studied the mechanical dynamics of additively produced lattices through FE analysis. In a comprehensive review they concluded that there is a significant mismatch between the understanding of the design process for additively manufactured lattice structures and the modelling of these parts, leading to inefficiencies in the design process. Physical testing validated by numerical analysis has also been undertaken by [12] who used optical analytics and FE modelling to study uniaxial loading and by [13] in a comprehensive study. Less conventional auxetic forms have been studied by [14] in a similar multi-format

approach concluding that “double-U” structures can reduce manufacturing damage and stress concentration under elastic loading.

3 Development of a novel testing configuration

3.1 Testing Setup

The main boundary condition problem has been addressed through the creation of a bespoke jig. Fig. 2 shows how the samples were mounted during testing. A series of adjustable pins were set into the sample on rails – this allowed both a small degree of movement but crucially held the sample firmly enough in order that the tension and compression forces could be applied. A basic lubricant was added to the rails to reduce the effects of friction. Taking inspiration from other research efforts (notably [7]) mounting points were set into the samples at uniformly distributed perimeter positions on all four sides. Recognising that there are clear benefits to both the optical analysis and a more technical mechanical analysis, our setup was configured to both record time lapsed images revealing displacements and to measure the mechanical forces. As shown in Fig. 2a, a high definition camera was placed above the sample, recording the physical changes in the structure. Sensitive force gauges were placed on two sides of the jig, recording real-time forces in the X and Y directions. Fig. 2c shows the final testing rig configuration.

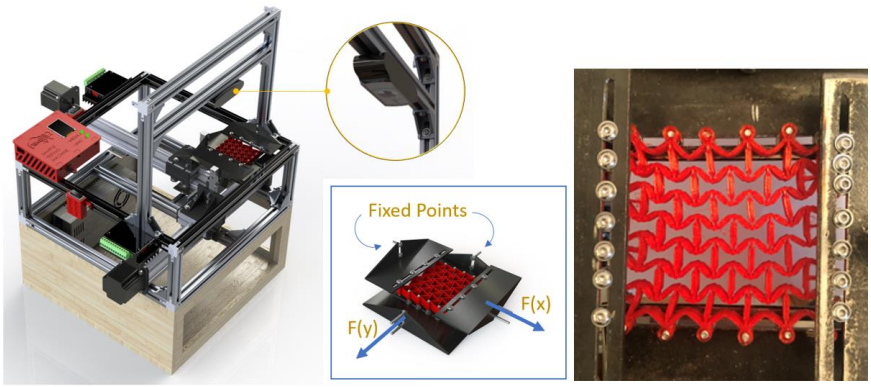

Fig. 2. Design of fully integrated testing rig with camera detail (a). Mounting design with support trusses and rails detail (b). Physical re-entrant sample mounted in testing jig (c).

3.2 Summary of key results

As this was the first run of test utilising this newly developed testing system, we decided to focus on conventional auxetic designs allowing us to thoroughly test the system with a set of well-understood structures. Fig. 1 shows the sample designs that we focused on; re-entrant, chiral and semi-rigid. Various design parameters were edited in CAD including the interior angle (IA) and the wall thickness (WT) and then printed in TPU using a FlashForge 3D printer. Each sample was 10 mm in depth. The results were

analysed by means of load-displacement curve, which are shown in Fig. 3 to 7. As a point of information, the graphs track a complete cycle from tension to compression.

3.2.1 Re-entrant sample tests

Much of the derived data produced consistent and usable results despite a difficult boundary condition setup. Starting with the lowest interior angle variable – 15 º, several results are of note when comparing these structures against their own variants in wall thickness and the other interior angle variants. For instance, Fig. 3 shows only small changes in recorded tension and compression forces at the two wall thickness extremes. This suggests that the largest overriding factor allowing the sample to sustain these loads may be the smaller interior angle, providing more mechanical freedom within the given deformation. There are some noted differences between the measured compressive forces, but this is only approximately 5-10 Newtons (N) across both axes.

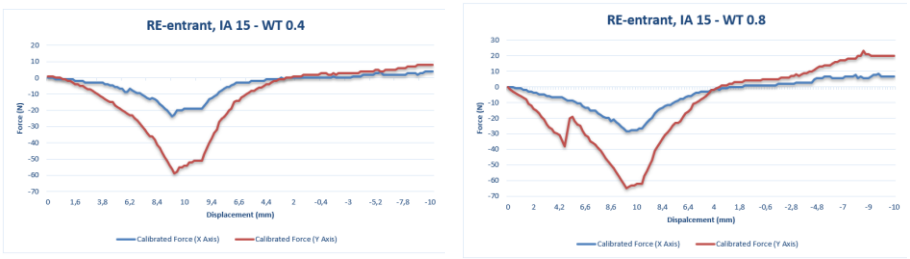

Fig. 3. Results of force-displacement study for two re-entrant structures characterized by different IA and WT.

If we now consider these in comparison to the other sample tests, some interesting conclusions can potentially be drawn. Fig. 4 shows the distinction between the recorded forces of the 0.8 mm wall thickness extreme for the re-entrant sample with a 20º interior angle as compared to 25º at 0.6 mm. Looking at the data for an interior angle of 25º, the lower recorded forces suggest even greater flexibility for that structure. Again, the higher wall thicknesses of this design led to marginally higher force readings as flexibility is reduced when compared with other tests (not shown for brevity).

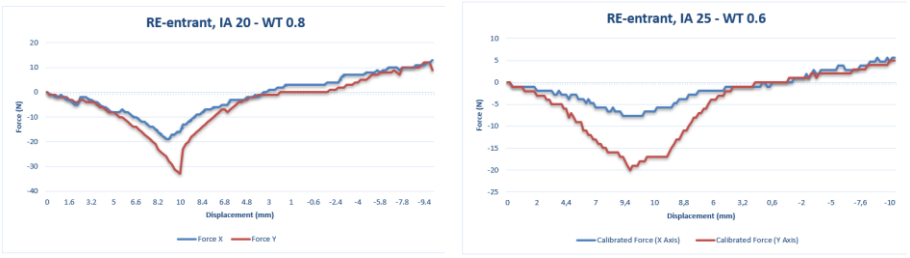

Fig. 4. Results of force-displacement study for two re-entrant structures characterized by different IA and WT.

3.2.2 Chiral sample tests

The chiral results differed from the re-entrant results in one distinct way since they showed greater uniformity in recorded mechanical behaviour across the X and Y axes. Again, the interior angles and the wall thicknesses of the build were varied. Considering the results at an interior angle of 60º, we can see a high level of uniformity in the recorded forces across both axes.

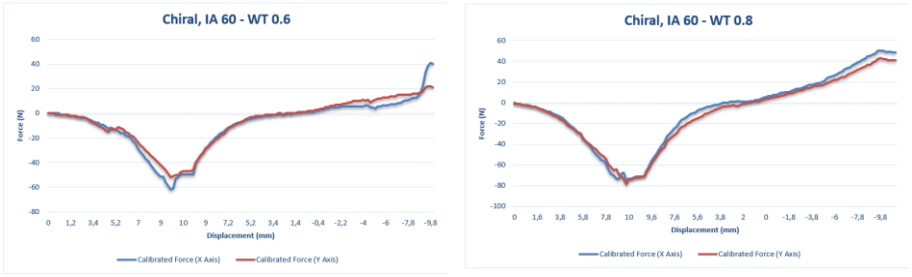

Fig. 5. Results of force-displacement study for two chiral structures characterized by different IA and WT.

A similar pattern is also seen with an increase in recorded forces as the wall thickness is increased. Interestingly, the results for the chiral samples show a distinctly larger increase in measured forces across both axes than the re-entrant samples. Fig. 5 shows an approximate increase by 20 N in tension and compression when different wall thicknesses are compared. When looking at a sample variant with a larger interior angle in Fig. 6, the recorded forces are reduced markedly when compared to the 60-degree sample (approximately 60 N) suggesting that these samples have a higher degree of mechanical flexibility, echoing the re-entrant results (Fig. 3 and 4). Interestingly however, doubling the wall thickness from 0.4 to 0.8 mm has a very large influence on the recorded forces, contrasting much of the re-entrant test data. Looking at Fig. 6 and comparing the graphs, a difference of about 60 N is recorded suggesting that this configuration is greatly affected by changes in wall profile, particularly in the tension phase.

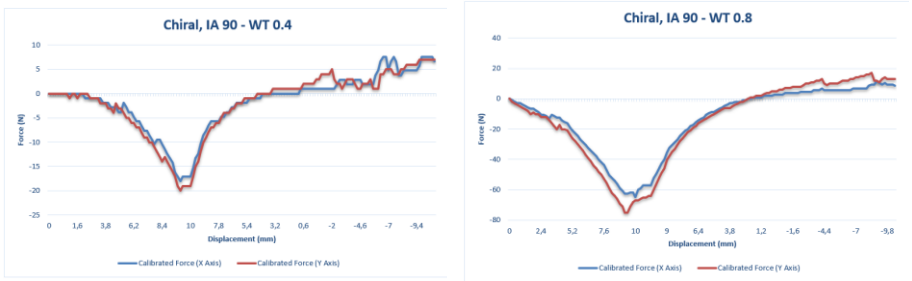

Fig. 6. Results of force-displacement study for two re-entrant structures characterized by different IA and WT.

To add more complexity to the discussion, the data for an interior angle of 120º record results very similar to that of the 90º samples with an increase in wall thickness hugely influencing the recorded forces although these results are not graphed for brevity. Only small differences are recorded when the parts are in compression, where a marginally larger compressive force is recorded for the larger 0.8 mm wall thickness. The similarities between the 90º and the 120º results (not shown) suggest that the interior angle above a certain threshold does not make a huge impact of the amount of force sustained by the sample as it is deformed.

3.2.3 Semi-rigid sample tests

The semi-rigid samples showed the same lack of uniformity as the re-entrant samples in terms of x/y behaviour but showed much greater recorded forces for both tension and compression when compared with most of the chiral and re-entrant sample variations. Considering the results shown in Fig. 7, it is clear how much force the samples are sustaining as they are deformed. This is mostly due to the increased rigidity of the samples due to their implicit geometric makeup, i.e. the samples are less skeletal and mostly solid compared to the chiral and re-entrant variants. While the chiral and re-entrant samples recoded forces at approximate maximums of 80 N, the semi-rigid samples sustained more than 100 N on the x-axis across the change in wall thickness, predictably showing greater flexibility with the smaller wall thickness. The higher compression forces show that the sample is becoming more structurally uniform as the material is pressed together – significantly more uniform than the chiral and re-entrant samples.

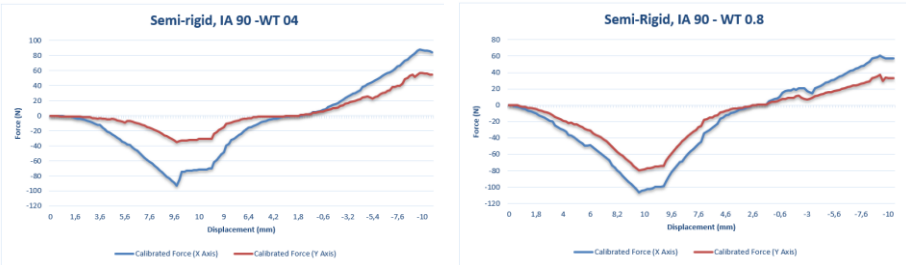

Fig. 7. Results of force-displacement study for two semi-rigid structures characterized by different IA and WT.

4 Simulation of mechanical behaviour

4.1 Finite element model

The simulations were performed with the add-in *simulation* of SolidWorks 2020. The mounting design, based on a series of pins trapped on a rail of the experimental testing rig, was modelled and reproduced by adopting a simplified approach. For constraining and loading the simulated auxetic structures, a cylinder (i.e. the pin) was used, and two

cubes were added at its top and bottom. The choice to utilize the cube was motivated by the possibility to have five free faces (one is attached to the cylinder) to constrain the auxetic structure on some axes and loading it on other axes. The method adopted is shown in Fig. 8a overleaf and a chiral structure is adopted as an example. The material applied to the auxetic structure was the same utilized for the experimental tests; TPU 95A. It was edited basing on the technical data sheet provided by the Ultimaker company (see https://ultimaker.com/materials/tpu-95a). The material applied to the fixtures, instead, was the AISI 316L. This was already included in the material library of SolidWorks and the choice was motivated by the requirement to use a stiffer material than TPU 95A for the fixtures. The simulation was run by using, for both materials, a linear elastic isotropic model with all the geometrical entities of the study treated as solid bodies. Finally, the mesh factor was set to "fine". This choice increased the calculation time, but it facilitated a higher accuracy in predicting the mechanical behaviour of the tested structure. All the auxetic structures characterized for the experimental tests (re-entrant, chiral and semi-rigid structures) were tested. For each type, one or two variants with a different interior angle or a different wall thickness were simulated. The magnitude of loads, for every single structure, was derived by the corresponding experimental test. Such an approach was adopted for comparing physical and virtual testing based on the respective displacement results. For each structure, the magnitude of the force applied was derived by using the load corresponding to the higher displacement (10 mm) measured during the experimental test. If the displacement of the virtual test was close to the one of the experimental tests, the simulations were validated, and the results considered robust. Finally, the results of simulations and experimental tests were also assessed by a qualitative visual comparison through observations of the deformation modes occurring.

4.2 Summary of key results

The simulations performed provided the charting of stress, displacement and strain. Fig. 8b shows the result obtained for the chiral structure (interior angle: 60°; wall thickness: 0.6 mm). In this case, the undeformed model was superimposed to the deformed shape for a more direct observation of the strain mode. The figure reports the linear displacement on the y-axis. It is close to the displacement that occurred for physically tested specimens (10 mm for x and y axes), under the same loading conditions and magnitude of the force (55 N on the x-axis and 54 N on the y-axis). The result was also confirmed for the chiral structure that, on the same loading and constraints conditions, the prediction of the displacement obtained through virtual test is reliable. Results obtained for the semi-rigid sample (interior angle: 60°; wall thickness: 0.8 mm) recorded a similar level of continuity between the physical behaviour and the simulated behaviour.

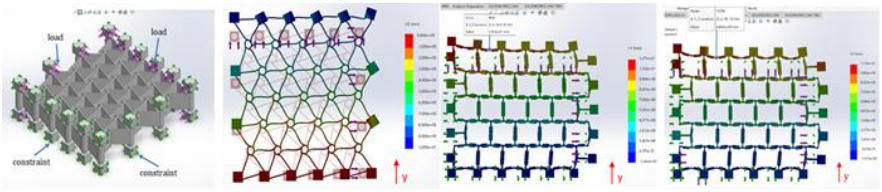

Fig. 8. Simulation setup with loads and constraints (a). Chiral structure (IA 60º; WT 0.6 mm), the undeformed is superimposed to the deformed result (b). Simulated result of re-entrant structure (IA 20º; WT 0.8 mm) (c). Simulated result of re-entrant structure (IA 25º; WT 0.6 mm) (d).

Fig. 8 also shows the displacement chart of the re-entrant structure with an interior angle of 20º and a wall thickness of 0.8 mm. The magnitude of the load set on the x-axis was 23 N and the magnitude on the y-axis was 34 N (analogous to the physical test). For this structure, the maximum displacement observed on the y-axis is larger than 10 mm. For the re-entrant structure an additional variant was simulated, with a different interior angle (25º) and wall thickness (0.6 mm). The magnitude of the loads applied is in this case was 7 N on the x-axis and of 19 N on the y-axis. The mechanical behaviour confirms the observations made for the variant, in both cases the displacement is close to a value of 10 mm, the peak is at the corner on the left and the strain mode is aligned with it. Fig. 9 shows a qualitative superimposed comparison between physical and virtual testing of chiral (a) and re-entrant structures (b) at 10 mm of displacement. The overlap between physical and virtual tests, in terms of displacement, was very good for both structures. However, it is to highlight that some slight deviations are present for the re-entrant structure, where on the horizontal axis the displacement is moderately larger for simulated structure compared to the experimental test.

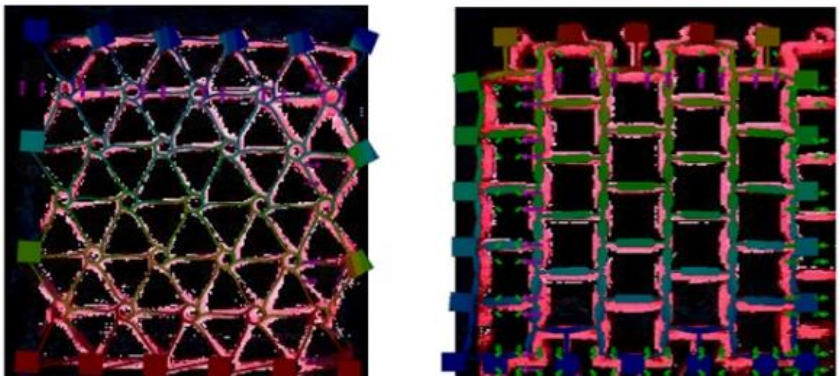

Fig. 9. Superimposed comparison between physical and virtual testing of chiral IA 60, WT 0.6 (a) and re-entrant IA 20, WT 0.8 (b) structures.

5 Discussion

From our initial analysis, we can derive a number of key results that we can discuss in this section. With respect to a more general conclusion, we can clearly show that all sample variations showed differences in recorded forces, demonstrating that interior angle geometry and wall thicknesses influence these mechanical behaviours. More specifically, it was shown that an increase in wall thickness always led to an increase in the recorded deformation forces indicating higher stiffnesses. A larger interior angle correlated strongly with a decrease in measured forces for chiral and re-entrant samples, suggesting that a smaller interior angle creates greater flexibility in the structure. With respect to the differences shown between the X and Y forces, large deviations were recorded for the re-entrant and semi-rigid samples but by contrast there is a close correlation in the chiral samples suggesting that the design facilitates behaviour that is more mechanically uniform. Differences in X/Y behaviour in re-entrant and semi-rigid samples is most likely due to the directional differences in geometry creating different mechanical effects. The chiral samples sustained greater forces than the re-entrant samples and semi-rigid samples sustained the largest forces of all the samples. Semi-rigid samples consistently sustained larger forces under compression than the re-entrant or chiral variants, most likely due to the material becoming denser and more uniform under compression. With respect to the simulation efforts, we showed a robust match between the physical and virtual behaviour of the auxetic structures under deformation and the results were aligned for all the tested geometries. The method proposed can be used not only for the validation of the auxetic structures, but also as a supporting tool for designing more optimized and advanced structures. Future work can be more focused on the study of stress distribution occurring when the auxetic structures are strained. This would facilitate the retrieval of useful information which could potentially drive critical design tasks such as material selection.

6 Conclusion

This work presents the results from a novel setup to mechanically test auxetic components with a view to unifying a number of testing approaches into one umbrella system. Even if the proposed setup was limited to “off-the-shelf” componentry, we sought to produce results similar to previous research efforts but provide novel solutions for the boundary condition question and unify particular methods such as optical analysis and force-displacement analysis. This paper presented the results from an initial study focusing on a range of small scale auxetic components. The data derived from the tests allowed for a number of conclusions to be drawn relating to the behaviour of auxetics of different build characteristics. These results were subsequently validated through finite element simulations. The close match between force-displacement analytics and the optical comparisons demonstrate the effectiveness and efficiency of the testing setup, and its ability to reproduce the desired constraint conditions. Future studies could address aspects such as fatigue behaviour occurring with cyclical loading and also consider stress distribution occurring when the auxetic structures are strained. With respect

to the design of auxetics, a testing setup such as ours presents the opportunity for the quick analysis of additively manufactured componentry that is both useful and reliable, stimulating the creation of more elaborate auxetic structures.

References

1. Lakes, R.: Foam Structures with a Negative Poissons Ratio. Science 235, 1038-1040 (1987)
2. Kolken, H.M.A., Zadpoor, A.A.: Auxetic mechanical metamaterials. Rsc Adv 7, 5111-5129 (2017)
3. Abdel-Rahman A., E.T.: Heat-Actuated Auxetic Facades. In: Facade Techtonics 2018 World Congress Los Angeles. (Year)
4. Zulifqar A., H.T., & Hu H.: Development of uni-stretch woven fabrics with zero and negative Poisson's ratio. Text Res J 88, 2076-2092 (2018)
5. Dubrovski, P.D., Novak, N., Borovinsek, M., Vesenjak, M., Ren, Z.R.: In-Plane Behavior of Auxetic Non-Woven Fabric Based on Rotating Square Unit Geometry under Tensile Load. Polymers-Basel 11, (2019)
6. Brighenti, R., Spagnoli, A., Lanfranchi, M., Soncini, F.: Nonlinear deformation behaviour of auxetic cellular materials with re-entrant lattice structure. Fatigue Fract Eng M 39, 599-610 (2016)
7. Auricchio, F., Bacigalupo, A., Gambarotta, L., Lepidi, M., Morganti, S., Vadala, F.: A novel layered topology of auxetic materials based on the tetrachiral honeycomb microstructure. Mater Design 179, (2019)
8. Jiang, L.L., Hu, H.: Finite Element Modeling of Multilayer Orthogonal Auxetic Composites under Low-Velocity Impact. Materials 10, (2017)
9. Alomarah, A., Masood, S.H., Sbarski, I., Faisal, B., Gao, Z.Y., Ruan, D.: Compressive properties of 3D printed auxetic structures: experimental and numerical studies. Virtual Phys Prototy 15, 1-21 (2020)
10. Ardebili, M.K., Ikikardaslar, K., Chauca, E., Delale, F.: Behavior of Soft 3d-printed Auxetic Structures under Various Loading Conditions. Proceedings of the Asme International Mechanical Engineering Congress and Exposition, 2018, Vol 9 (2019)
11. *removed for review*
12. Li, X., Wang, Q.S., Yang, Z.Y., Lu, Z.X.: Novel auxetic structures with enhanced mechanical properties. Extreme Mech Lett 27, 59-65 (2019)
13. Yang, C., Vora, H.D., Chang, Y.: Behavior of auxetic structures under compression and impact forces. Smart Mater Struct 27, (2018)
14. Yang, H., Wang, B., Ma, L.: Mechanical properties of 3D double-U auxetic structures. Int J Solids Struct 180, 13-29 (2019)